IRIS AperTO

UNIVERSITÀ DEGLI STUDI DI TORINO

AperTO - Archivio Istituzionale Open Access dell'Università di Torino

The Role of Iron Impurities in the Toxic Effects Exerted by Short Multiwalled Carbon Nanotubes (MWCNT) in Murine Alveolar Macrophages.

This is the author's manuscript

Original Citation:

Availability:

This version is available http://hdl.handle.net/2318/140669 since

Published version:

DOI:10.1080/15287394.2013.834855

Terms of use:

Open Access

Anyone can freely access the full text of works made available as "Open Access". Works made available under a Creative Commons license can be used according to the terms and conditions of said license. Use of all other works requires consent of the right holder (author or publisher) if not exempted from copyright protection by the applicable law.

(Article begins on next page)

25 August 2022

UNIVERSITÀ DEGLI STUDI DI TORINO

This is an author version of the contribution published on:
Questa è la versione dell'autore dell'opera:

Journal of Toxicological and Environmental Health Part A, 76(18), 2013, doi:

10.1080/15287394.2013.834855

The definitive version is available at:
La versione definitiva è disponibile alla URL:
http://www.tandfonline.com/doi/abs/10.1080/15287394.2013.834855?url_ver=Z39.88-2003&rfr_id=ori:rid:crossref.org&rfr_dat=cr_pub%3dpubmed#.UysLALdOVMs

Aldieri E.*‡, Fenoglio I.†‡, Cesano F.†‡, Gazzano E.*‡, Gulino G.*‡, Scarano D.†‡, Attanasio A.§, Mazzucco G.§, Ghigo D. *‡, Fubini B. †‡.

The role of iron impurities in the toxic effects exerted by short MWCNT in murine alveolar macrophages.

* Department of Oncology, University of Torino, Via Santena 5/bis, Torino, 10126 Torino, Italy.

† Department of Chemistry, University of Torino, Via P. Giuria 7, 10125 Torino, Italy.

‡ Interdepartmental Centre "G. Scansetti" for Studies on Asbestos and other Toxic Particulates, University of Torino, Italy.

§ Department of Medical Sciences, Via Santena 7, University of Torino, 10126 Torino, Italy.

Corresponding author: Elisabetta Aldieri, Department of Oncology, Via Santena 5/bis, 10126 Torino, Italy. Phone: +39-011-6705844. Fax: +39-011-6705845. E-mail: elisabetta.aldieri@unito.it

ABSTRACT

Lung toxicity mediated by multiwalled carbon nanotubes (MWCNT) has been widely demonstrated and recently associated with induction of carcinogenic asbestos-like effects, but the chemical features which drive this toxic effect have still not been well elucidated. The presence of metals as trace contaminants during MWCNT preparation, in particular iron (Fe) impurities, plays an important role in determining a different cellular response to MWCNT. Our goal was to clarify the mechanisms underlying MWCNT toxicity in correlation to the presence of Fe impurities by exposing murine alveolar macrophages to two different MWCNT samples, which differ only for the presence or absence of Fe. Data show that only Fe-rich MWCNT were significantly cytotoxic, genotoxic and induced a potent cellular oxidative stress, while Fe-free MWCNT did not exert any of these toxic effects. These results confirm that Fe content represents a very important key constituent in promoting MWCNT induced toxicity, and this needs to be taken into consideration when planning new, safer, preparation routes.

Running Title: The role of impurities in MWCNT toxicity.

Keywords: multiwalled carbon nanotubes, iron, physico-chemical properties, lung toxicity.

INTRODUCTION

Multiwalled carbon nanotubes (MWCNT) have many industrial applications (Endo et al., 2008). This has promoted studies to investigate the potential toxic effects upon occupational or environmental exposure. MWCNT exposure has been strongly associated to lung toxicity and its effects have been compared to asbestos-induced carcinogenesis (Jaurand et al., 2009; Pacurari et al., 2010; Guo et al., 2012). MWCNT are cytotoxic and induced oxidative stress (Shvedova et al., 2012), in particular in human lung epithelial (A549) cells (Choi et al., 2009; Herzog et al., 2009), normal human primary bronchial epithelial (NHBE) cells (Herzog et al., 2009), human lung fibroblasts (Wang et al., 2010), and human bronchial epithelial (BEAS-2B) cells (Hirano et al., 2010). Moreover MWCNT were also shown to exert genotoxic effects in cultured Chinese hamster lung cells (Asakura et al., 2010) and A549 cells (Kato et al., 2012). A MWCNT-induced pulmonary toxicity was also observed in *in vivo* studies: in mice MWCNT exposure was associated with relevant oxidative lung damage, both after intratracheal instillation (Aiso et al., 2010; Reddy et al., 2010 a or b) or pleural penetration (Mercer et al., 2010), and in ICR mice Kato et al. (2012) a significant genotoxic effect exerted by MWCNT after intratracheal instillation was noted.

MWCNT-related adverse effects were also observed in tissues different from the lung. Hu et al. (2010) showed cytotoxic effects in keratinocytes and T helper lymphocytes, Migliore et al. (2010) reported an oxidative stress in the murine macrophage cell line RAW 264.7, Patlolla et al. (2010) reported cytotoxic, genotoxic and pro-apoptotic effects exerted in human dermal fibroblasts. Finally Reddy et al. (2010 a or b) provided evidence of increased cytotoxic and oxidative stress in HEK293 human embryonic kidney cells. More recently, Han et al. (2012) confirmed this MWCNT-induced toxicity in C6 rat glioma cells, and Kato et al. (2012) in Chinese hamster ovary AA8 cells, with particular reference to DNA damage.

These adverse effects have been related to the MWCNT physico-chemical features (Oberdörster, 2010) but little is known regarding the role as possible mediators of oxidative stress. MWCNT are produced with different physico-chemical properties, depending upon the method of synthesis and post-synthetic modifications, that alter their characteristics and toxicity in a variable way (Fenoglio et al., 2008; Muller et al., 2008; Liu et al., 2012).

Metallic contaminants were demonstrated to play a role in MWCNT-mediated toxicity (Bello et al., 2009) and metal trace impurities increased the levels of reactive oxygen species (ROS) in rat NR8383 macrophages and human A549 lung cells (Pulskamp et al., 2007). In particular, the iron (Fe) state and content needs to be considered as a determinant in driving the adverse effects exerted by MWCNT. This topic has been widely developed with asbestos fibers, whose related induced oxidative stress and cytotoxicity have been clearly associated (Aust et al., 2011) to Fe activity. It is well known how asbestos fibers generate free radicals via different mechanisms including a Fenton reaction catalyzed by Fe ions exposed to their surface (Kamp, 2009). Our research group showed a correlation between the coordination and oxidation state of Fe in asbestos and its toxicity in *in vitro* cellular systems (Aldieri et al., 2001; Gazzano et al., 2007; Turci et al., 2010). It is thus conceivable to postulate a role for Fe also in MWCNT-induced toxic effects.

Some studies have been performed on single wall carbon nanotubes (SWCNTs) with varying Fe content. In RAW 264.7 macrophages the presence of Fe in SWCNTs was crucial in eliciting significant loss of reduced glutathione and accumulation of lipid hydroperoxides (Kagan et al., 2006; Wang et al., 2010). On the other hand, Haniu et al. (2010) showed with a proteomic approach that in human monoblastic leukemia (U937) cells the cytotoxic effect of MWCNT depended on their impurities, since the adverse effects attributed to MWCNT were lost after thermal treatment (producing Fe depletion) of the particles. The intratracheal

instillation of Fe-depleted MWCNT induced less severe acute inflammation compared to pristine MWCNT in murine lungs (Kim et al., 2010).

To better elucidate the mechanism of MWCNT-mediated toxicity, straights were undertaken to investigate in alveolar macrophages the effects of MWCNT only differing in the state and abundance of Fe.

MATERIALS and METHODS.

Preparation of Fe-rich and Fe-free MWCNT.

MWCNT were produced from commercial pristine MWCNT purchased from Mitsui Chemicals (Kawasaki-Shi, Japan) by catalytic chemical vapor deposition (CVD) production method (via the floating reactant/catalyst technique of organic precursors and ferrocene). Pristine MWCNT were heated up to 2400 °C in air flow for 15 min and then ground in an oscillatory agate ball mill (Pulverisette 0, Fritsch) with a vertical vibration of 1 mm applied during 6 h. To remove metals, one aliquot of ground MWCNT was suspended in 1 M HCl and the suspension stirred at 25°C for 10 days. The MWCNT were recovered by centrifugation 13000 g, washed with distilled water and dried.

Surface area. The surface area of MWCNT was measured by means of the Brunauer–Emmett–Teller (BET) method based on N_2 adsorption at -196°C by using an automatic instrument (ASAP 2010, Micromeritics, Norcross, GA) on a representative amount of powder. The powder has been degassed at 150°C prior the measurement.

Morphology. The dimension of MWCNT was evaluated directly by means of transmission electron microscopy (TEM). The statistical evaluation of diameters and lengths of the MWCNT fragments was obtained by considering a population of 213 data each, from low

resolution TEM images (4000-25000x). The structure and the morphology of the MWCNT before and after the removal of Fe were also evaluated by HRTEM analysis. TEM images were collected by a JEOL 3010-UHR TEM instrument operating at 300 kV.

Purity. The purity of the pristine MWCNT was investigated by thermogravimetric analyses air flow (ramp, 10°C/min) by a TA instrument Q600 SDT Simultaneous DSC-TGA heat flow analyser.

Elemental analysis. The elemental composition was quantified after complete calcination at 800°C of 10 mg of MWCNT and re-suspension of the residue in 5 mL of 37% HCl in MilliQ water. The concentration of contaminants was quantified in the solution after dilution in MilliQ water by atomic emission-inductively coupled plasma (AE-ICP) spectrometry (IRIS II Advantage/1000, Thermo Jarrel Ash, Franklin, MA).

Evaluation of potentially bioavailable iron. This test was performed to evaluate the amount of Fe ions exposed at the surface of the MWCNT according to a procedure described previously (Martra et al., 2003; Liu et al., 2008). For this purpose, a strong Fe^{2+} ions chelator (ferrozine) and a reducing agent (ascorbic acid) were used to extract Fe ions. Twenty-five mg of the powders were incubated in 10 ml of a 3 mM solution of ascorbic acid and ferrozine. After 10 days an aliquot of the supernatant was withdrawn after centrifugation 13000 g and the concentration of Fe evaluated by measuring the absorbance at 562 nm (typical of the complex ferrozine-Fe(II)) with an UV/Vis spectrophotometer (Uvikon, Kontron, Eching, Germany).

Raman Spectroscopy. Micro-Raman spectra were acquired using an integrated micro/macro Raman system which includes a Horiba Jobin Yvon HR800 microspectrometer, an Olympus BX41 microscope and a CCD air-cooled detector. A polarized solid state Nd 80 mW laser operating at 532.11 nm was used as the excitation source. Calibration of the instruments was performed by measuring the Stokes and anti-Stokes bands and checking the position of the Si band at ± 520.7 cm^{-1}. Each spectrum was acquired using a 100X objective, resulting in a laser beam size at the sample in the order of 2 mm. To optimize the signal to noise ratio, spectra were acquired using 10 scans of 10 sec for each spectral region. In order to produce strong signals without inducing surface alteration due to the heat, a filter with optical density d = 0.6 was used. The software LabSpec 5 (Horiba Jobin Yvon) was used to analyze the spectra. The I_D/I_G value is the ratio of the intensities of two bands designated as D (1340 cm^{-1}) and G (1570 cm^{-1}) which correspond respectively to structural defects and to the tangential in-plane stretching vibration of the carbon-carbon bonds within the graphene sheets.

Free radical generation. The ability of a particle to generate radical species was monitored by electron spin resonance (ESR) spectroscopy (Miniscope 100 ESR spectrometer, Magnettech, Berlin, Germany) using the spin trapping technique with 5,5-dimethyl-1-pyrroline-N-oxide (DMPO) as trapping agent according to a procedure described by Fenoglio et al. (2006). A typical reaction is the generation of $HO^{\bullet}$ radicals from hydrogen peroxide through a Fenton-like reaction (Fubini and Hubbard, 2003). DMPO was purchased from Alexis (Lausen, Switzerland), the other reagents from Sigma-Aldrich (St. Louis, MO). A suspension of 5 mg of MWCNT in 50 µl of 5% sodium dodecyl-sulphate (SDS) was diluted in 125 µl of a buffered solution (0.2 M potassium phosphate buffer, pH 7.4) containing 68 mM DMPO and 45 mM hydrogen peroxide. The ESR spectra were recorded directly on an aliquot of the suspension within one hr.

The experiments were also repeated on the supernatant, after removal of nanotubes: 15 mg of Fe-rich MWCNT were suspended in 375 μl of 0.2 M potassium phosphate buffer, pH 7.4. The suspension was stirred for 60 min and then MWCNT were removed by centrifugation 13000 g. To 125 μl of the solution 375 μl of a buffered solution (0.2 M potassium phosphate buffer, pH 7.4) containing 75 mM DMPO and 50 mM hydrogen peroxide were then added. The ESR spectra were recorded within one hr. All experiments were repeated at least twice.

Scavenging activity toward hydroxyl radicals. The activity was monitored by ESR according to the procedure previously employed for MWCNT (Fenoglio et al., 2006-2008). Hydroxyl ($HO^{\bullet}$) radicals were generated by irradiating directly in the ESR spectrophotometer cavity (Thermo Oriel UV-lamp, Stratford, CT) a buffered solution (0.05 M potassium phosphate buffer, pH 7.4) containing 27 mM DMPO and 9 mM hydrogen peroxide. The concentration of $HO^{\bullet}$ radicals was followed by measuring the intensity of the ESR spectrum of the DMPO/$HO^{\bullet}$ adduct (g = 2.006; a^N =14.4 G a^H =14.3 G). The reaction was repeated in the presence of a suspension of 5 mg of MWCNT in 50 μl of 5% SDS. All the experiments were repeated at least twice.

Dispersion of MWCNT in the culture media. The MWCNT samples were suspended in the culture media described below at the concentration of 260 mg/ml. The suspensions were sonicated for 2 min twice (100 W, 20 kHz, Sonoplus, Bandelin, Berlin, Germany).

Average hydrodynamic size of MWCNT in the culture media was evaluated by means of dynamic light scattering (DLS) (Zetasizer Nano-ZS, Malvern Instruments, Worcestershire, UK). The measurement was repeated after 15 min to evaluate the stability of the suspension. Since in the DLS technique particles larger than 6 μm are not detected, optical microscopy (DFC295, Leica, 100x) was also used to detect the presence of large aggregates.

Cells and reagents. Murine alveolar macrophages (MH-S) were provided by Istituto Zooprofilattico Sperimentale "Bruno Ubertini" (Brescia, Italy). Cells were cultured in 35 (1.2 x 10^6 cells) or 100 mm-diameter Petri dishes (7.5 x 10^6 cells) in RPMI-1640 + 10% fetal bovine serum (FBS) up to confluence, and then incubated for 24 hr in the absence or presence of Fe-rich or Fe-free MWCNT (25-100 µg/cm^2) before the assays, or with 25 µg/cm^2 UICC (Union International Contre le Cancer) crocidolite asbestos fibers, used as a positive control of toxicity. MWCNT and crocidolite fibers were sonicated (100 W: 2 min MWCNT, 30 sec crocidolite) (Labsonic Sonicator; Sartorius Stedim Biotech S.A., Aubagne, France) before incubation with cell cultures to allow better suspension in the culture medium.

The protein content of the monolayers and cell lysates was assessed with the BCA kit from Pierce (Rockford, IL). Plasticware was from Falcon (Becton Dickinson, Franklin Lakes, NJ). Unless otherwise specified, other reagents were purchased from Sigma-Aldrich.

Measurement of leakage of lactate dehydrogenase (LDH) activity. The cytotoxic effect of MWCNT was measured as leakage of LDH activity into the extracellular medium (Riganti et al., 2002). After each incubation, the extracellular medium was collected and centrifuged at 13000 x g for 30 min. The cells (cultured in 35 mm-diameter Petri dishes, 1.2 x 10^6 cells) were washed with fresh medium, detached with trypsin/EDTA (0.05/0.02% v/v), washed with PBS, resuspended in 1 ml of TRAP (82.3 mM triethanolamine, pH 7.6), and sonicated on ice with two 10 sec bursts. Aliquots of cell lysate (5 µl, 2.5 µg protein) and of extracellular medium (50 µl/2 ml medium) were diluted with TRAP and supplemented with 0.5 mM sodium pyruvate and 0.25 mM NADH (final volume of the mix, 300 µl) to start the reaction. The reaction was followed for 10 min, measuring the absorbance at 340 nm (37°C) with a Packard EL340 microplate reader (Bio-Tek Instruments, Winooski, VT). Each reaction

kinetics was linear throughout the time of measurement. Both intracellular and extracellular enzyme activities were expressed as µmol of NADH oxidized/min/dish, and then extracellular LDH activity (LDH out) was calculated as a % total (intracellular + extracellular) LDH activity (LDH tot) in the dish.

Measurement of lipid peroxidation. TBARS (thiobarbituric acid-reactive substances) assay, used to detect the lipid peroxidation products, was performed according to Yano (1988). After 24 hr incubation in the absence or presence of different MWCNT concentrations, cells (cultured in 60 mm-diameter Petri dishes, 2.5 x 10^6 cells) were washed with fresh medium, detached with trypsin/EDTA (0.05/0.02%, v/v), and resuspended in 1 ml PBS. A 500 µl aliquot of cell suspension, each containing the same amount of cell proteins (0.1 mg), was added to 5 µl of Triton X-100 and 500 µl of TBA solution (0.375% thiobarbituric acid and 30% trichloroacetic acid in 0.5 N HCl). Samples were boiled for 20 min at 100°C, rapidly cooled by immersion in an ice bath, and centrifuged for 30 sec at 13000 g. The absorbance of 300 µl of the reaction mixture at 532 nm was read with a Packard EL340 microplate reader. TBARS values were expressed as pmol/mg cellular protein.

Measurement of intracellular glutathione. Intracellular reduced glutathione (GSH) was measured as previously described (Vandeputte et al., 1994). The cells (cultured in 35 mm-diameter Petri dishes, 1.2 x 10^6 cells) were washed with PBS, and 600 µl 0.01 N HCl was added to each cell monolayer. After scraping, the cells were frozen/thawed twice and proteins precipitated by adding 120 µl of 6.5% 5-sulfosalicylic acid to 480 µl lysate. Each sample was placed in ice for 1 hr and centrifuged for 15 min at 13000 g (4°C). The total GSH was measured in 20 µl of the cell lysate (15 µg protein) with the following reaction mix: 20 µl stock buffer (143 mM NaH_2PO_4, 63 mM EDTA, pH 7.4), 200 µl daily reagent (10 mM 5,5′-

dithiobis-2-nitrobenzoic acid (DTNB), 2 mM NADPH in stock buffer), 40 µl glutathione reductase (8.5 U/mL). The kinetics of reaction was followed at 415 nm for 10 min (to check that it was linear) using a Packard microplate reader EL340. Each measurement was made in triplicate, results expressed as nmol of GSH/mg cellular protein.

Western blotting. Cells (from 100 mm-diameter Petri dishes, 7.5 x 10^6 cells) were directly solubilized in a lysis buffer (25 mM HEPES, 135 mM NaCl, 1% NP40, 5 mM EDTA, 1 mM EGTA, 1 mM $ZnCl_2$, 50 mM NaF, 10% glycerol), supplemented with a protease inhibitor cocktail set III (100 mM AEBSF, 80 µM aprotinin, 5 mM bestatin, 1.5 mM E-64, 2 mM leupeptin, and 1 mM pepstatin; Calbiochem-Novabiochem Corporation, San Diego, CA), 2 mM phenylmethylsulfonyl fluoride and 1 mM sodium orthovanadate. Heme oxygenase 1 (HO-1) protein (32 kDa) and GAPDH protein (37 kDa) were separated by SDS-PAGE (12%) (10 µg protein), transferred to a polyvinylidene difluoride (PVDF) membrane sheet and probed with the rabbit anti-HO-1 antibody (D.B.A. Italia s.r.l., Milan, Italy), diluted 1:1000 in PBS-BSA 1%, and/or anti-GAPDH (Santa Cruz Biotechnology, Santa Cruz, CA), diluted 1:500 in PBS-BSA 1%. After overnight incubation, the membrane was washed with PBS-Tween 0.1% and subjected for 1 hr to a peroxidase-conjugated anti-rabbit IgG (sheep, Amersham International, Bucks, UK) (diluted 1:1000 in PBS-Tween with Blocker Non-Fat Dry Milk 5%, Biorad). The membrane was washed again with PBS-Tween 0.1% and proteins were detected by enhanced chemiluminescence (PerkinElmer, Shelton, CT).

Alkaline comet assay. Single-cell gel electrophoresis (comet assay) was performed under alkaline conditions according to the method of Singh et al. (1988) with slight modifications. All steps were performed under dim yellow light to prevent additional DNA damage. 7.5 µl cell suspension (5 x 10^4 cells) was mixed with 75 µl low melting point agarose (0.8%) and

placed on the clear part of a frosted microscope slide precoated with a layer of normal melt point agarose (1%) and low melting point agarose. Then, slides were immersed in lysis buffer for 1 hr (4°C, 2.5 M NaCl, 0.1 M Na_2EDTA, 10 mM Tris, 0.5% N-laurylsarcosine, supplemented with 1% Triton X-100 just before use). To perform the DNA unwinding, slides were placed in a horizontal electrophoresis unit containing the electrophoresis buffer (300 mM NaOH, 1 mM Na_2EDTA, pH >13) for 40 min. Alkaline electrophoresis was performed in the same buffer for 20 min (25 V, 300 mA). Slides were washed thrice with neutralization buffer (0.4 M Tris, pH 7.5) and then they were dehydrated in 70% ethanol (5 min) and left to dry, allowing the storage until analysis. To analyze DNA damage, slides were stained with DAPI (10 µg/ml, 5 min). Fifty randomly chosen, non-overlapping comets per comet slide were observed using a Leica fluorescence microscope (20X objective) and an image analysis system (CometScore, TriTek Corp. Sumerduck, VA).

Uptake of MWCNT. To assess the actual internalization of the MWCNT into the cells, Trasmission Electron Microscopy (TEM) was used. Cells were plated in 100 mm Petri dishes (7.5×10^6 cells) and cultured, then incubated for 24 hr in the absence or presence of 50 µg/cm^2 of Fe-rich MWCNT, 50 µg/cm^2 of Fe-free MWCNT and 25 µg/cm^2 of crocidolite asbestos. After this incubation, cells were washed with PBS, detached, and fixed with 2.5% 0.1 M glutaraldehyde in cacodylate buffer pH 7.4 for 15 min, postfixed with 1% osmium tetroxide for 3 hr, dehydrated in graded ethanol, treated with propylene oxide, and embedded in epoxy-resin. Ultrathin sections were collected on Formvar-coated grids, stained with uranyl acetate and lead citrate, and examined with TEM (Philips CM10, Amsterdam, The Netherlands).

Statistical Analysis. All data in text and figures are provided as means ± SEM. The results were analyzed by a one-way Analysis of Variance (ANOVA) and Tukey's test. $p < 0.05$ was considered significant.

RESULTS.

Preparation of iron-rich and iron-free MWCNT.

The MWCNT consisting in straight tubes of 5-10 μm with a mean diameter of 65-70nm (Table 1) were selected for the low amount of the amorphous carbon and for their high-crystallinity high-purity together with the absence of catalytic supports (Cravotto et al., 2011). These properties come from the CNT production method (CVD) and from the subsequent thermal annealing. As the CNT tend to form large aggregate in culture media, pristine MWCNT were ground in an agate ball mill. In Figure 1a the TEM images of ground MWCNT are shown. This treatment reduced the length of nanotubes to less than 4 μm (Table 1). Pristine MWCNT contain 0.5% Fe and 0.03% Al as impurities derived from the catalyst that were used during the synthesis. By using a specific chelator for Fe(II) associated to a reducing agent iron was found in large part exposed to the solvent and therefore potentially active toward cells (Table 1). Several protocols were proposed to remove metal contaminants from MWCNT (Cho et al., 2009), that include chemical treatments with oxidizing acids (HNO_3, H_2SO_4) or thermal treatments at high temperature in inert atmosphere (Bougrine et al., 2001; Fenoglio et al., 2008). However these treatments also affect the total amount of defects of CNT. Since defects were found to modulate the toxicity of CNT (Muller et al., 2008, Fenoglio et al., 2008), the use of these protocols would not allow to investigate the role of Fe impurities. Therefore a mild treatment consisting in the incubation of MWCNT in an aqueous solution of diluted HCl at room temperature (Cao et al., 2008) was used. This treatment removes Fe leaving unaltered the degree of defects and functionalities present in the

ground samples (Cao et al., 2008). As expected, in our sample the Fe impurities were almost completely removed following this treatment (Table 1) without altering the microscopic structure of the nanotubes, as evidenced by TEM (Figure1a-b) and Raman spectroscopy (Table 1).

Dispersion of MWCNT in cellular media.

Being highly hydrophobic, MWCNT are not well dispersed in aqueous media. However, the presence of proteins were reported to stabilize the suspension of CNT (Sager et al., 2007; Elgrabli et al., 2007). For this reason MWCNT were dispersed by mild sonication directly in the cellular media containing fetal calf serum. The degree of dispersion and the stability of the suspensions were evaluated by means of DLS (Figure 2a). A single peak, corresponding to particles having an equivalent hydrodynamic diameter of 353 nm was detected. The Polydispersion index (PDI) was of 0.35 indicating a wide agglomerate size distribution. Since DLS technique has an upper limit of 6 μm, the presence of larger aggregates was evaluated by optical microscopy (Figure 2b). MWCNT appeared uniformly distributed in the suspension with some aggregates having a diameter of 1-5 μm. The stability of the suspension was followed for a time period of 15 minutes, which is largely sufficient for a correct dosage. No changes were detectable both in form and position of the peak.

Generation and/or scavenging of free radicals and ROS.

When tested for their potential to generate free radicals and ROS in aqueous suspension in the presence of hydrogen peroxide, all samples, as already reported for other MWCNT (Fenoglio et al., 2006, 2008), failed to generate any form of radical detectable by means of the ESR/spin trapping technique (Figure 3a-b). However, when the tests were repeated on the supernatant obtained by incubating Fe-rich MWCNT in phosphate buffer and then removing MWCNT by

centrifugation, a clear signal corresponding to $HO^{\bullet}$ radicals was observed suggesting that, under these conditions, MWCNT partially released Fe ions are able to catalyze the generation free radicals. The lack of this signal in the presence of MWCNT may thus be attributed to a scavenging activity of MWCNT toward these radical species. To further confirm this hypothesis $HO^{\bullet}$ radicals were generated via a Fenton reaction in the presence of MWCNT following a previously adopted procedure (Fenoglio et al., 2006, 2008). As expected in the presence of both MWCNT samples the ESR signal corresponding to $HO^{\bullet}$ radicals completely disappeared.

4. Iron-rich MWCNT-induced cytotoxicity.

After incubation with Fe-rich MWCNT, MH-S cells showed a significantly increased release of LDH, used as sensitive index of cytotoxicity, in a concentration-dependent manner (Figure 4a). This toxic effect exerted by Fe-rich MWCNT exposure was hardly detectable when MH-S cells were incubated with equal amounts of Fe-free MWCNT (Figure 4a). From the results obtained, in the subsequent experiments with MH-S the 50 $\mu g/cm^2$ concentration was used, as representative of an acute toxic damage. The incubation of MH-S cells with crocidolite asbestos, used as a positive control of cytotoxicity, as expected induced a significant leakage of LDH in MH-S cells (Figure 4a).

Iron-rich MWCNT evoked indices of oxidative stress.

After incubation with Fe-rich MWCNT, MH-S cells showed a significantly augmented accumulation of TBARS, used as index of oxidative stress induction (Figure 4b), which was absent in MH-S cells incubated with Fe-free MWCNT (Figure 4b). The incubation with crocidolite asbestos induced an oxidative stress under our experimental conditions in MH-S cell line (Fig 4b).

The level of GSH, the most important intracellular antioxidant molecule, is a sensitive index of the efficiency of cellular antioxidant defences. After incubation with Fe-rich MWCNT, MH-S cells showed a significantly decreased intracellular GSH levels (Figure 4c) which was not observed when the cells were incubated with Fe-free MWCNT (Fig 4c). Exposure to crocidolite produced an intracellular GSH depletion in MH-S cell line (Figure 4c).

The expression of HO-1, an enzyme involved in heme catabolism, whose level increases after an oxidative stress was also investigated in MH-S cells (Sandau et al., 1998). After incubation of MH-S cells with Fe-rich MWCNT, HO-1 showed a significantly elevated expression (Figure 5a-b), similarly to cells exposed to crocidolite asbestos, but this induction was not observed in MH-S cells incubated with Fe-free MWCNT (Figure 5a-b). The expression of GAPDH was used as a control of equal protein loading and showed no difference (Figure 5a-b).

Genotoxicity induction.

To verify if the toxicity exerted by Fe-rich MWCNT may be related to a genotoxic effect, following the incubation in the above mentioned conditions the MH-S cells were subjected to single-cell gel electrophoresis (comet assay) (Table 2). Three indices of DNA damage were recorded: tail length (measured from the middle of the comet to the end of the tail), tail DNA (% DNA in the tail) and tail moment (= tail length x tail DNA). All these indicators were significantly higher in MH-S cells incubated with Fe-rich MWCNT or crocidolite in comparison with control cells or MH-S cells incubated with Fe-free MWCNT (Table 2).

Internalization of MWCNT.

To evaluate if the different adverse effects exerted by Fe-free and Fe-rich MWCNT were a consequence of a different uptake of CNT by macrophages, TEM analysis was performed on

MH-S cells incubated in the absence or presence of Fe-rich MWCNT, Fe-free MWCNT or crocidolite fibers (Figure 6). Cells showed a similar internalization of both Fe-free and Fe-rich MWCNT (Figure 6b-c), as well as crocidolite fibers (Figure 6d). Agglomerates of different size were observed inside the cells for both MWCNT samples, while no single MWCNT were observed. Agglomerates were mainly localized in the cytoplasm. MWCNT were not observed in the nucleus or in other organelles.

DISCUSSION.

Although numerous studies examined the possible adverse effects of MWCNT, many questions are still open, particularly those related to understanding the role of physico-chemical properties. Pristine MWCNT may be contaminated by catalyst remnants (usually Fe, Al, Co, Ni, or Mo), which appear as metal residues at the surface of the MWCNT (Bello et al., 2009). Among these metallic impurities, few investigators correlated the presence of Fe in CNT to their toxic and/or pro-inflammatory effects (Kagan et al., 2006; Haniu et al., 2010; Kim et al., 2010). CNT synthesis remains costly and difficult, due to the high temperatures and pressures required, and there does not exist consensus on preparation of CNT (grinding, impurity removal, etc.). However, the CVD procedure used in this work has proved to be the most suitable synthesis process for the production of CNT with controlled characteristics, such as diameter, length and number of walls (Kumar and Ando, 2010), although challenges of the process are currently addressed with future directions.

In the present study, two different types of MWCNT differing only with respect to content in Fe and similar in diameter, length and defectivity were prepared and tested for their toxicity toward MH-S cells.

Fe-rich MWCNT exerted a significant cytotoxic effect, measured as LDH release, in mouse MH-S alveolar macrophages, in a concentration-dependent manner, while no marked

cytotoxic effect was observed after exposure to Fe-free MWCNT. Actually, concentrations tested were relatively higher than those used in animal models. On the other hand, the toxicity of Fe-containing MWCNT has been widely shown. Instead, our aim was to investigate whether Fe-free MWCNT are toxic or not: for this reason, we tested high doses of Fe-free MWCNT in order to rule out their in vitro toxicity.

Since LDH leakage is strictly related to a cellular membrane damage, which may result from an oxidative stress, both MWCNT samples were examined for their ability to produce lipoperoxidation, GSH consumption and HO-1 induction in MH-S cells. Again, only Fe-rich MWCNT, and not Fe-free samples, induced significant signs of oxidative stress.

These results suggest a key role played by Fe impurities in the MWCNT-induced cellular oxidation. Experiments performed in a cell-free system showed that both Fe-rich and Fe-free MWCNT samples failed to generate any detectable free radical, but both capable to scavenge hydroxyl radicals, confirming previous studies (Fenoglio et al., 2006, 2008; Crouzier et al., 2010). The Fe impurities contained in the Fe-rich sample were shown to be highly bioavailable and potentially reactive. Therefore they may potentially dissolve in the intracellular milieu and induce oxidative stress. Since MWCNT were shown to be scavengers of hydroxyl radicals, one may argue that they mitigate the Fe-induced oxidative stress in the cells, which otherwise would appear more potent.

The effects of MWCNT in MH-S cells also affected DNA, since only Fe-rich MWCNT exerted a genotoxic effect, by inducing a strong DNA fragmentation which was absent after incubation of MH-S cells with Fe-free MWCNT.

The observed toxic effect exerted by Fe-rich MWCNT is hardly due to a different uptake of CNT since MH-S cells internalized in the same way Fe-free and Fe-rich MWCNT. This result provides further evidence to our hypothesis that the different Fe % in MWCNT is the main constituent responsible for the adverse effects observed.

Data suggest that Fe plays an important role in the toxicity of MWCNT. This is only apparently related to that observed for asbestos fibers (Aust et al., 2011; Turci et al., 2010). In fact a strict correlation between the presence of Fe at the surface of different types of asbestos fibers in a well-defined redox and coordination state (crocidolite, chrysotile) and related toxicity was previously demonstrated (Aldieri et al., 2001; Gazzano et al., 2007). However, while in asbestos fibers iron is contained inside the crystal framework, in the case of CNT metallic contaminants are mainly in the form of metallic or metal oxide clusters or nanoparticles. Furthermore, while iron is always exposed at the surface of asbestos, in CNT the metals may be both exposed to the solvent contact, as in the present case, or embedded inside the tube (Fubini et al., 2011). Only in the first case they may be released thus contributing to the observed toxic effects. The present data are consistent with those obtained by Kagan et al. (2006) with SWCNT, and also with the results from Haniu et al. (2010) and Kim et al. (2010), showing a correlation between Fe content and MWCNT pro-inflammatory effects.

Since the Fe content in MWCNT represents a key point in promoting cytotoxicity, oxidative stress and DNA damage, it should be important to remove Fe impurities from MWCNT during their preparation, in an attempt to produce a material safer for public health and nanomedicine applications.

Acknowledgements.

This work was supported by the Regione Piemonte (CIPE 2006 project “NANOSAFE”), by the Compagnia San Paolo.

Declaration of Interest.

The authors declare that there are no conflicts of interest.

REFERENCES.

- Aiso, S., Yamazaki, K., Umeda, Y., Asakura, M., Kasai, T., Takaya, M., Toya, T., Koda, S., Nagano, K., Arito, H. and Fukushima, S. 2010. Pulmonary toxicity of intratracheally instilled multiwall carbon nanotubes in male Fischer 344 rats. *Ind. Health.*, 48**:**783-795.

- Aldieri, E., Ghigo, D., Tomatis, M., Prandi, L., Fenoglio, I., Costamagna, C., Pescarmona, G., Bosia, A. and Fubini, B. 2001. Iron inhibits the nitric oxide synthesis elicited by asbestos in murine macrophages. *Free Radic. Biol. Med.*, 31:412-417.

- Asakura, M., Sasaki, T., Sugiyama, T., Takaya, M., Koda, S., Nagano, K., Arito, H. and Fukushima, S. 2010. Genotoxicity and cytotoxicity of multi-wall carbon nanotubes in cultured Chinese hamster lung cells in comparison with chrysotile A fibers. *J. Occup. Health.*, 52:155-166.

- Aust, A. E., Cook, P. M. and Dodson, R. F. 2011. Morphological and chemical mechanisms of elongated mineral particle toxicities. *J. Toxicol. Environ. Health B*, 14:40-75.

- Bello, D., Wardle, B. L., Yamamoto, N., Guzman deVilloria, R., Garcia, E. J., Hart, A. J., Ahn, K., Ellenbecker, M. J. and Hallock, M. 2009. Exposure to nanoscale particles and fibers during machining of hybrid advanced composites containing carbon nanotubes. *J. Nanopart. Res.*, 11:231-249.

- Bougrine, A., Dupont-Pavlovsky, N., Naji, A., Ghanbaja, J., Mareche, J. F. and Billaud, D. 2001. Influence of high temperature treatments on single-walled carbon nanotubes structure, morphology and surface properties. *Carbon*, 39:685-695.

- Cao, L. C., Liu, Y. Q., Wang, Y., Wei, D. C., Fu, L., Hu, P. A., Zhang, H. L., Huang, L. P. and Yu, G. 2008. Wet purification of aligned carbon nanotube arrays and its impact on the morphology of the carbon nanotube arrays. *Acta Physico-Chim Sinica*, 24:951-954.

- Cho, H. G., Kim, S. W., Lim, H. J., Yun, C. H., Lee, H. S. and Park, C. R. 2009. A simple and highly effective process for the purification of single-walled carbon nanotubes synthesized with arc-discharge. *Carbon*, 47: 3544-3549.

- Choi, S. J., Oh, J. M. and Choy, J. H.2009. Toxicological effects of inorganic nanoparticles on human lung cancer A549 cells. *J. Inorg. Biochem.*, 103:463-471.

- Cravotto, G., Garella, D., Gaudino, E. C., Turci, F., Bertarione, S., Agostini, G., Cesano, F. and Scarano, D. 2011. Rapid purification/oxidation of multi-walled carbon nanotubes under 300 kHz-ultrasound and microwave irradiation. *New J. Chem.,* 35:915-919.

- Crouzier, D., Follot, S., Gentilhomme, E., Flahaut, E., Arnaud, R., Dabouis, V. and Debouzy, J. C. 2010. Carbon nanotubes induce inflammation but decrease the production of reactive oxygen species in lung. *Toxicology*, 272:39-45.

- Elgrabli, D., Abella-Gallart, S., Aguerre-Chariol, O., Robidel, F., Rogerieux, F., Boczkowski, J. and Lacroix, G. 2007. Effect of BSA on carbon nanotube dispersion for in vivo and in vitro studies. *Nanotoxicology*, 1:266-278.

- Endo, M., Koyama, S., Matsuda, Y., Hayashi, T. and Kim, Y. A. 2005. Thrombogenicity and blood coagulation of a microcatheter prepared from carbon nanotube - Nylon-based composite. *Nano Letters*, 5:101-105.

- Fenoglio, I., Tomatis, M., Lison, D., Muller, J., Fonseca, A., Nagy, J. B. and Fubini, B. 2006. Reactivity of carbon nanotubes: free radical generation or scavenging activity? *Free Radic. Biol. Med.*, 40:1227-1233.

- Fenoglio, I., Greco, G., Tomatis, M., Muller, J., Raymundo-Pinero, E., Beguin, F., Fonseca, A., Nagy, J. B., Lison, D. and Fubini, B. 2008. Structural defects play a major role in the acute lung toxicity of multiwall carbon nanotubes: Physicochemical aspects. *Chem, Res. Toxicol.*, 21:1690-1697.

- Fubini, B. and Hubbard, A. 2003. Reactive oxygen species (ROS) and reactive nitrogen species (RNS) generation by silica in inflammation and fibrosis. *Free Radic. Biol. Med.*, 34:1507-1516.

- Fubini, B., Fenoglio, I., Tomatis, M. and Turci, F. 2011. Effect of chemical composition and state of the surface on the toxic response to high aspect ratio nanomaterials. *Nanomedicine*, 6:899-920.

- Gazzano, E., Turci, F., Foresti, E., Putzu, M. G., Aldieri, E., Silvagno, F., Lesci, I. G., Tomatis, M., Riganti, C., Romano, C., Fubini, B., Roveri, N. and Ghigo, D. 2007. Iron-loaded synthetic chrysotile: A new model solid for studying the role of iron in asbestos toxicity. *Chem. Res. Toxicol.*, 20:380-387.

- Guo, N. L., Wan, Y-W., Denvir, J., Porter, D. W., Pacurari, M., Wolfarth, M. G., Castranova, V. and Qian, Y. 2012. Multiwalled carbon nanotubes-induced gene signatures in the mouse lung: Potential predictive value for human lung cancer risk and prognosis. *J. Toxicol. Environ. Health A*, 75:1129-1153.

- Han, Y., Xu, J., Li, Z., Ren, G. and Yang, Z. 2012. In vitro toxicity of multi-walled carbon nanotubes in C6 rat glioma cells. *Neurotoxicology*, 33:1128-1134.

- Haniu, H., Matsuda, Y., Takeuchi, K., Kim, Y. A., Hayashi, T. and Endo, M. 2010. Proteomics-based safety evaluation of multi-walled carbon nanotubes. *Toxicol. Appl. Pharmacol.*, 242:256-262.

- Herzog, E., Byrne, H. J., Davoren, M., Casey, A., Duschl, A. and Oostingh, G. J. 2009. Dispersion medium modulates oxidative stress response of human lung epithelial cells upon exposure to carbon nanomaterial samples. *Toxicol. Appl. Pharmacol.*, 236: 276-281.

- Hirano, S., Kanno, S. and Furuyama, A. 2010 Multi-walled carbon nanotubes injure the plasma membrane of macrophages. *Toxicol. Appl. Pharmacol.*, 249:8-15.

- Hu, X., Cook, S., Wang, P., Hwang, H. M., Liu, X. and Williams, Q. L. 2010. In vitro evaluation of cytotoxicity of engineered carbon nanotubes in selected human cell lines. *Sci. Total Environ.*, 408:1812-1817.

- Jaurand, M. C., Renier, A. and Daubriac, J. 2009. Mesothelioma: Do asbestos and carbon nanotubes pose the same health risk? *Part. Fibre Toxicol.*, 12:6-16.

- Kagan, V. E., Tyurina, Y. Y., Tyurin, V. A., Konduru, N. V., Potapovich, A. I., Osipov, A. N., Kisin, E. R., Schwegler-Berry, D., Mercer, R., Castranova, V. and Shvedova, A. A. 2006. Direct and indirect effects of single walled carbon nanotubes on RAW 264.7 macrophages: Role of iron. *Toxicol. Lett.*, 165:88-100.

- Kamp, D. W. 2009. Asbestos-induced lung diseases: An update. *Transational Research.: the journal of laboratory and clinical medicine*, 153: 43-152.

- Kato, T., Totsuka, Y., Ishino, K., Matsumoto, Y., Tada, Y., Nakae, D., Goto, S., Masuda, S., Ogo, S., Kawanishi, M., Yagi, T., Matsuda, T., Watanabe, M. and Wakabayashi, K. 2012. Genotoxicity of multi-walled carbon nanotubes in both in vitro and in vivo assay systems. *Nanotoxicology*, 7:452-461.

- Kim, J. E., Lim, H. T., Minai-Tehrani, A., Kwon, J. T., Shin, J. Y., Woo, C. G., Choi, M., Baek, J., Jeong, D. H., Ha, Y. C., Chae, C. H., Song, K. S., Ahn, K. H., Lee, J. H., Sung, H. J., Yu, I. J., Beck, G. R. Jr. and Cho, M. H. 2010. Toxicity and clearance of intratracheally administered multiwalled carbon nanotubes from murine lung. *J. Toxicol. Environ. Health A*, 73:1530-1543.

- Kumar, M. and Ando, Y. 2010. Chemical vapor deposition of carbon nanotubes: a review on growth mechanism and mass production. *J. Nanosci. Nanotech.*, 10:3739-3758.

- Liu, X., Guo, L., Morris, D., Kane, A. B. and Hurt, R. H. 2008. Targeted removal of bioavailable metal as a detoxification strategy for carbon nanotubes. *Carbon NY*, 46:489-500.

- Liu, D., Wang, L., Wang, Z. and Cuschieri, A. 2012. Different cellular response mechanisms contribute to the length-dependent cytotoxicity of multi-walled carbon nanotubes. *Nanoscale Research Letters*, 7:361.

- Martra, G., Tomatis, M., Fenoglio, I., Coluccia, S. and Fubini, B. 2003. Ascorbic acid modifies the surface of asbestos: possible implications in the molecular mechanisms of toxicity. *Chem. Res. Toxicol.*, 16:328-335.

- Mercer, R. R., Hubbs, A. F., Scabilloni, J. F., Wang, L., Battelli, L. A., Schwegler-Berry, D., Castranova, V. and Porter, D. W. 2010. Distribution and persistence of pleural penetrations by multi-walled carbon nanotubes. *Part. Fibre Toxicol.*, 4:7-28.

- Migliore, L., Saracino, D., Bonelli, A., Colognato, R., D'Errico, M. R., Magrini, A., Bergamaschi, A. and Bergamaschi, E. 2010. Carbon nanotubes induce oxidative DNA damage in RAW264.7 cells. *Environ. Mol. Mutagen.*, 51:294-303.

- Muller, J., Huaux, F., Fonseca, A., Nagy, J. B., Moreau, N., Delos, M., Raymundo-Piñero, E., Béguin, F., Kirsch-Volders, M., Fenoglio, I., Fubini, B. and Lison, D. 2008. Structural defects play a major role in the acute lung toxicity of multiwall carbon nanotubes: Toxicological aspects. *Chem. Res. Toxicol.*, 21:1698-1705.

- Oberdörster, G. 2010. Safety assessment for nanotechnology and nanomedicine: Concepts of nanotoxicology. *J. Intern. Med.*, 267:89-105.

- Pacurari, M., Castranova, V. and Vallyathan, V. 2010. Single- and multi-wall carbon nanotubes versus asbestos: Are the carbon nanotubes a new health risk to humans? *J. Toxicol. Environ. Health A*, 73:378-395.

- Patlolla, A., Knighten, B. and Tchounwou, P. 2010. Multi-walled carbon nanotubes induce cytotoxicity, genotoxicity and apoptosis in normal human dermal fibroblast cells. *Ethnicity and disease*, 20:65-72.

- Pulskamp, K., Diabaté, S. and Krug, H. F. 2007. Carbon nanotubes show no sign of acute toxicity but induce intracellular reactive oxygen species in dependence on contaminants. *Toxicol. Lett.*, 168:58-74.

- Reddy, A. R., Reddy, Y. N., Krishna, D. R. and Himabindu, V. 2010a. Pulmonary toxicity assessment of multiwalled carbon nanotubes in rats following intratracheal instillation. *Environ. Toxicol.*, 27:211-219.

- Reddy, A. R., Reddy, Y. N., Krishna, D. R. and Himabindu, V. 2010b. Multi wall carbon nanotubes induce oxidative stress and cytotoxicity in human embryonic kidney (HEK293) cells. *Toxicology*, 272:11-16.

- Riganti, C., Aldieri, E., Bergandi, L., Fenoglio, I., Costamagna, C., Fubini, B., Bosia, A. and Ghigo, D. 2002. Crocidolite asbestos inhibits pentose phosphate oxidative pathway and glucose 6-phosphate dehydrogenase activity in human lung epithelial cells. *Free Radic. Biol. Med.*, 32:938-949.

- Sager, T. M., Porter, D. W., Robinson, V. A., Lindsley, W. G., Schwegler-Berry, D. E. and Castranova, V. 2007. Improved method to disperse nanoparticles for in vitro and in vivo investigation of toxicity. *Nanotoxicology*, 1:118-129.

- Sandau, K., Pfeilschifter, J. and Brüne, B. 1998. Nitrosative and oxidative stress induced heme oxygenase-1 accumulation in rat mesangial cells. *Eur. J. Pharmacol.*, 342:77-84.

- Singh, N. P., McCoy, M. T., Tice, R. R. and Schneider, E. L. 1988. A simple technique for quantitation of low levels of DNA damage in individual cells. *Exp. Cell. Res.*, 175:184-191.

- Shvedova, A. A., Pietroiusti, A., Fadeel, B., Kagan, V. E. 2012. Mechanisms of carbon nanotube-induced toxicity: focus on oxidative stress. *Toxicol. Appl. Pharmacol.*, 261:121-133.

- Turci, F., Tomatis, M., Lesci, I. G., Roveri, N. and Fubini, B. 2010. The iron-related molecular toxicity mechanism of synthetic asbestos nanofibres: a model study for high-aspect-ratio nanoparticles. *Chemistry*, 17:350-358.

- Vandeputte, C., Guizon, I., Genestie-Denis, I., Vannier, B. and Lorenzon, G. 1994. A microtiter plate assay for total glutathione and glutathione disulfide contents in cultured/isolated cells: performance study of a new miniaturized protocol. *Cell. Biol. Toxicol.*, 10:415-421.

- Wang, L., Mercer, R. R., Rojanasakul, Y., Qiu, A., Yongju, L., Scabilloni, J. F., Wu, N. and Castranova, V. 2010. Direct fibrogenic effects of dispersed single-walled carbon nanotubes on human lung fibroblasts. *J. Toxicol. Environ. Health A*, 73:410-422.

- Yano, E. 1988. Mineral fiber-induced malondialdehyde formation and effects of oxidant scavengers in phagocytic cells. *Int. Arch. Occup. Environ. Health*, 61:19-23.

FIGURES CAPTIONS.

Fig. 1 TEM images of: a) MWCNT and b) iron-free MWCNT. Both kinds of carbon nanotubes have a high crystallinity, however the local presence of fractures and defects may be observed. In the insets, low resolution TEM images are reported. The nanotubes appear straight and hundred nanometres long.

Fig. 2 Dispersion of MWCNT (260 mg/ml) in RPMI +10% FCS: a) equivalent hydrodynamic diameter of single MWCNT or agglomerates evaluated by means of DLS. The lines correspond to five measurements conducted during 15 minutes. b) Optical micrograph of the suspension.

Fig. 3 Oxidative potential and scavenging activity of MWCNT. Panel a) ESR spectra registered on the suspension of Fe-rich or Fe-free MWCNT in a buffered solution (phosphate buffer 0.2 M, pH 7.4) of 48 mM DMPO and 32 mM H_2O_2 compared to the ESR spectra registered on the supernatant (Fe-rich MWCNT sup) obtained after incubation of Fe-rich MWCNT in phosphate buffer for 1 hour and removal of MWCNT by centrifugation. The ESR signal observed on the supernatant (spectrum a, a^N =14.4 G a^H =14.3 G) corresponds to the radical $HO^{\bullet}$. Panel b) Effect of MWCNT on the amount of $HO^{\bullet}$ radicals generated through photolysis of H_2O_2. The ESR signal observed in the absence of MWCNT (no MWCNT) corresponds to the radical $HO^{\bullet}$. No signal has been observed in the presence of Fe-rich or Fe-free MWCNT, suggesting a scavenging activity of these particles.

Fig. 4 Effect of Fe-rich MWCNT and Fe-free MWCNT on LDH leakage (panel a), TBARS (thiobarbituric acid-reactive substances) production (panel b) and GSH intracellular level (panel c) in MH-S cells: MH-S cells were incubated for 24 h in the absence (CTRL) or presence of 25, 50 or 100 μg/cm^2 of Fe-rich MWCNT (MWCNT) or Fe-free MWCNT [MWCNT (– Fe)] or crocidolite fibers (CRO, 25 μg/cm^2), used as positive control. Cells were then washed, detached and checked

for LDH activity (a), TBARS determination (b) and GSH intracellular level (c). Data are presented as means ± SEM (n = 6). Vs CTRL: * $p < 0.005$; ** $p < 0.001$. Vs MWCNT: • $p < 0.05$.

Fig. 5 Effect of Fe-rich MWCNT and Fe-free MWCNT on HO-1 protein expression in MH-S cells: a) Cells were incubated for 24 h in the absence (CTRL) or presence of 50 μg/cm^2 of Fe-rich MWCNT (MWCNT) or Fe-free MWCNT [MWCNT (– Fe)] or crocidolite fibers (CRO, 25 μg/cm^2), used as positive control. After a 24 h incubation, the cellular extracts were analysed by Western blotting with an anti-HO-1 and anti-GAPDH (used as a control of equal protein loading) antibody, as indicated under Materials and Methods. Each figure is representative of three experiments with similar results. b) Relative band intensities, calculated from all results described in the upper panel, were obtained using ImageJ software (http://rsb.info.nih.gov/ij/) and expressed as arbitrary units (mean ± SEM, n = 3). Vs CTRL : *$p < 0.001$; versus MWCNT: • $p < 0.01$.

Fig. 6 MWCNT internalization: representative TEM micrographs of MH-S cells incubated for 24 h in the absence (a) or presence of 50 μg/cm^2 of Fe-rich MWCNT (b), 50 μg/cm^2 of Fe-free MWCNT (c) or 25 μg/cm^2 of crocidolite asbestos (d). The white area surrounding the MWCNTs aggregates is due to the rupture of the resin used to embed the cells during the preparation of thin sections.

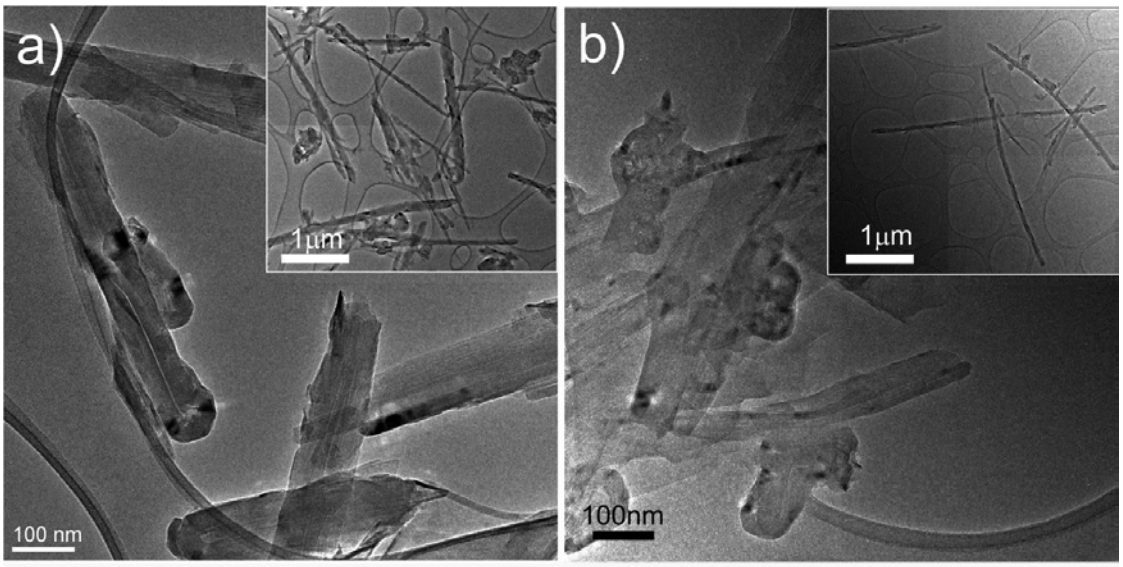

Fig. 1

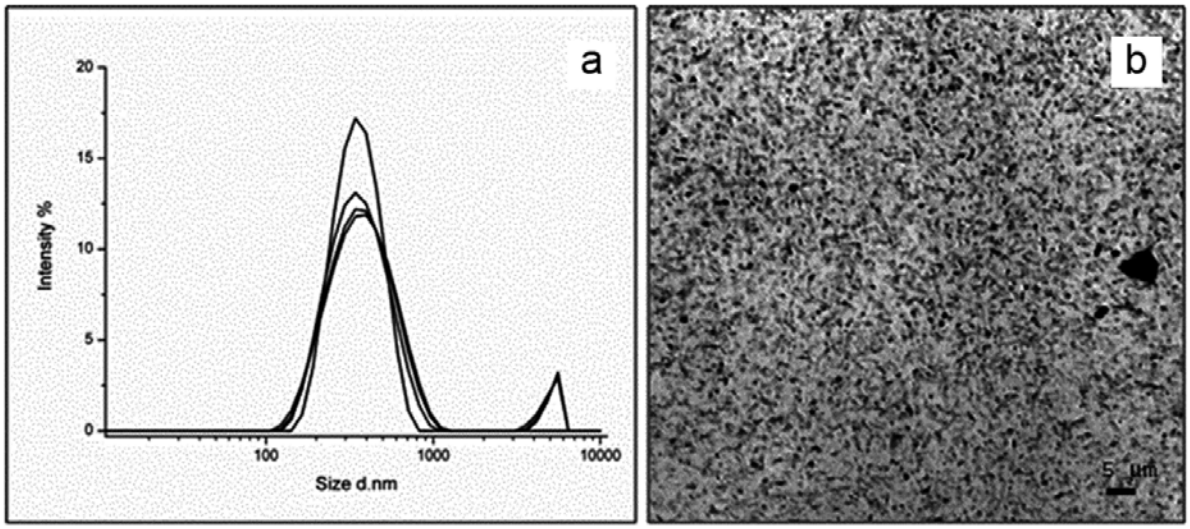

Fig. 2

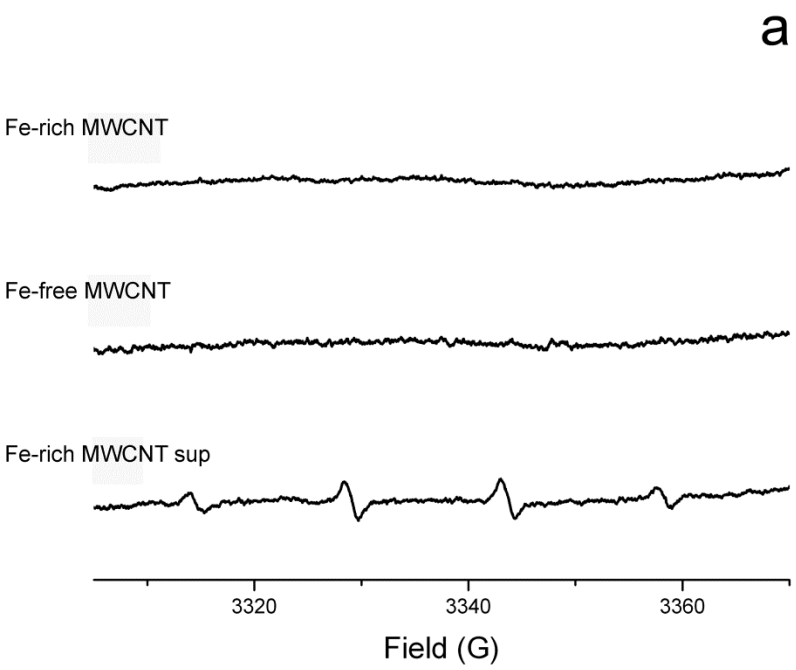
a
Fe-rich MWCNT
Fe-free MWCNT
Fe-rich MWCNT sup
3320
3340
3360
Field (G)

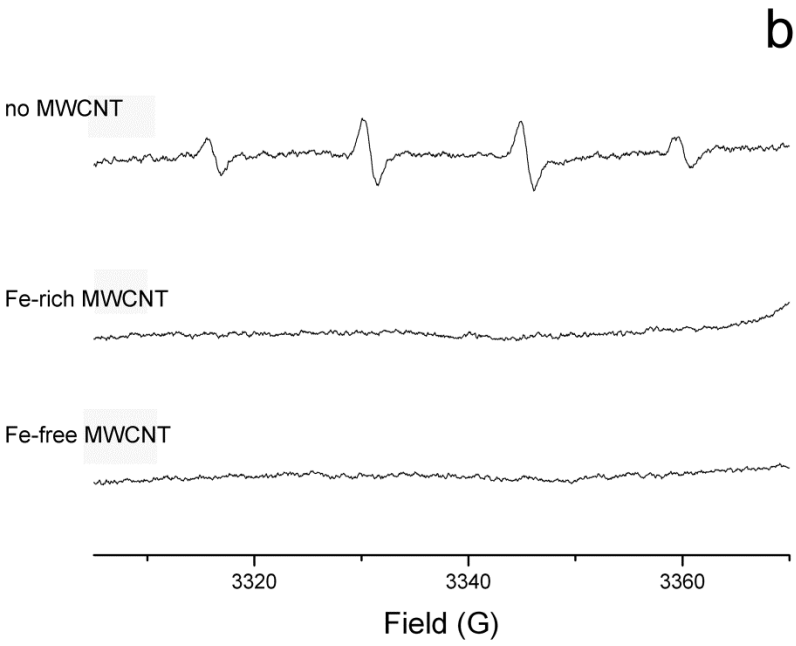
b
no MWCNT
Fe-rich MWCNT
Fe-free MWCNT
3320
3340
3360
Field (G)

Fig. 3

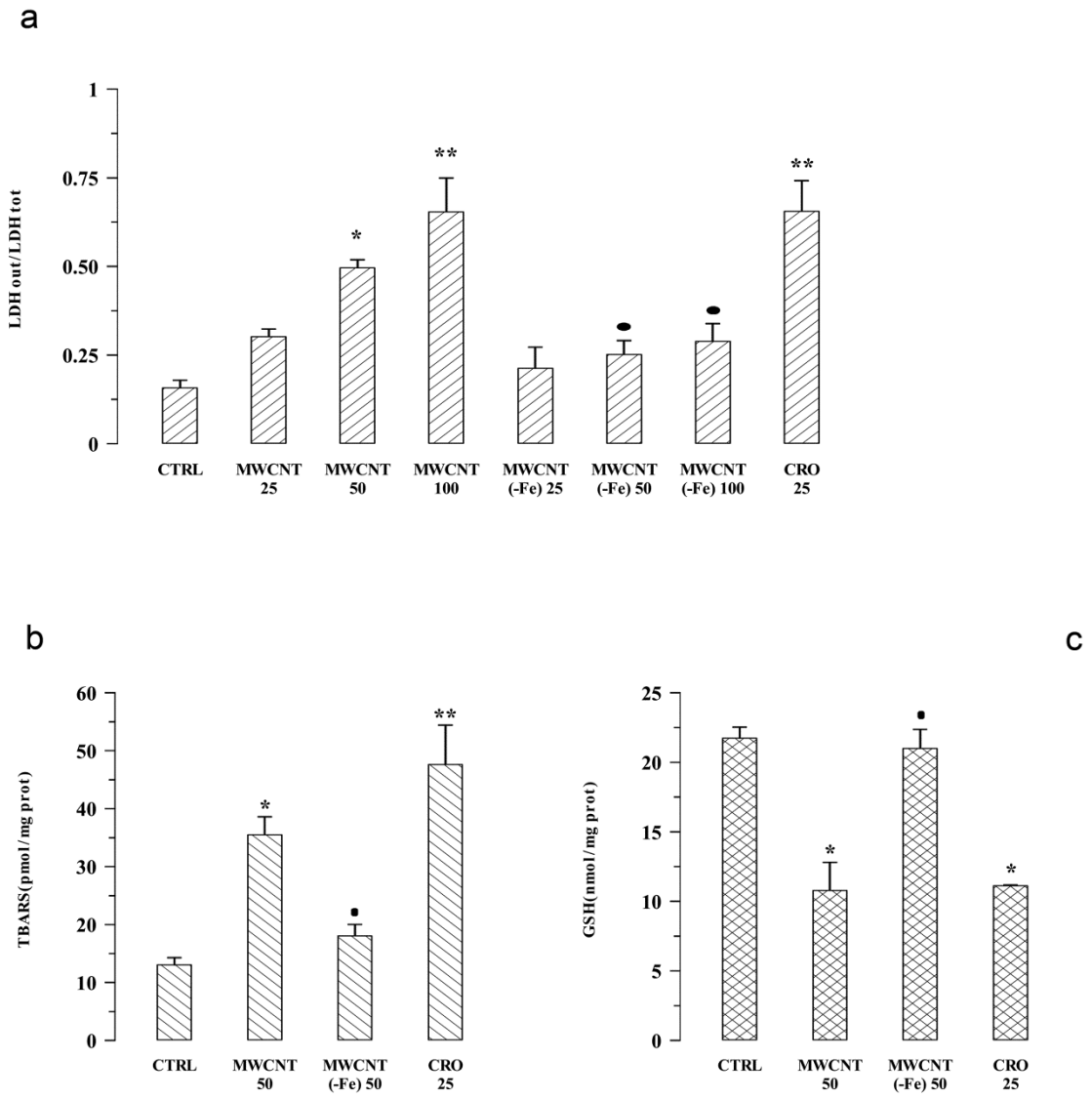
a
LDH out/LDH tot
1
0.75
0.50
0.25
0
CTRL
MWCNT 25
MWCNT 50
MWCNT 100
MWCNT (-Fe) 25
MWCNT (-Fe) 50
MWCNT (-Fe) 100
CRO 25
b
TBARS(pmol/mg prot)
60
50
40
30
20
10
0
CTRL
MWCNT 50
MWCNT (-Fe) 50
CRO 25
c
GSH(nmol/mg prot)
25
20
15
10
5
0
CTRL
MWCNT 50
MWCNT (-Fe) 50
CRO 25

Fig. 4

a

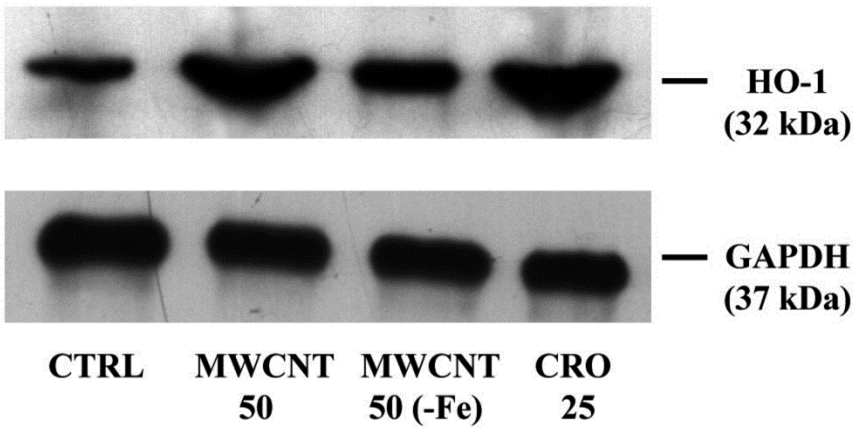
HO-1
(32 kDa)
GAPDH
(37 kDa)
CTRL
MWCNT 50
MWCNT 50 (-Fe)
CRO 25

b

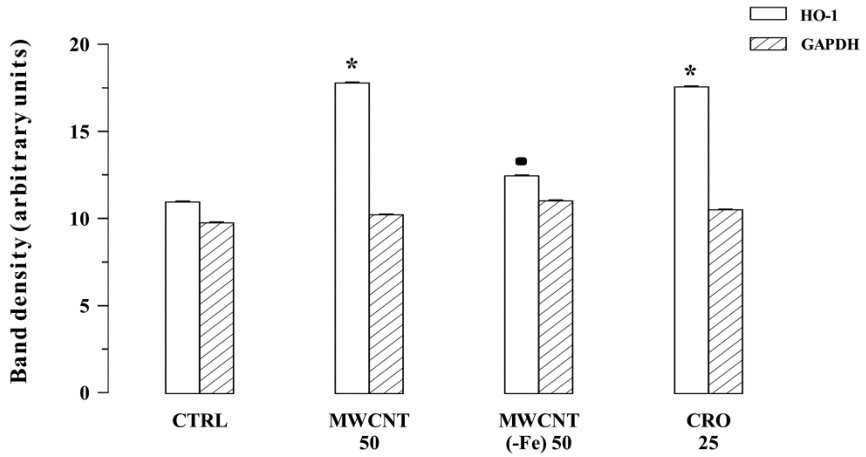
HO-1
GAPDH
Band density (arbitrary units)
20
15
10
5
0
*
*
CTRL
MWCNT 50
MWCNT (-Fe) 50
CRO 25

Fig. 5

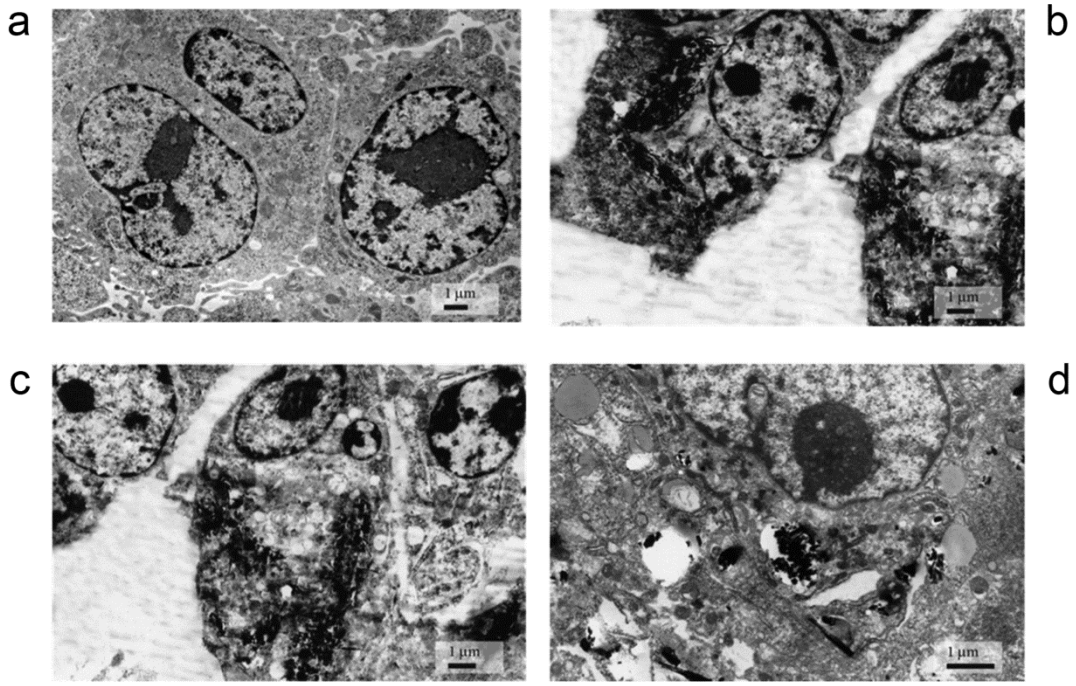

Fig. 6